Supplemental Information

Astrocyte-microglia interaction drives evolving neuromyelitis optica lesion

Tingjun Chen[1], Vanda A. Lennon[1,2], Yong U. Liu[1], Dale B. Bosco[1], Yujiao Li[1], Min-Hee Yi[1], Jia Zhu[1], Shihui Wei[3] and Long-Jun Wu[1,2,4*]

[1] Department of Neurology, Mayo Clinic, Rochester, MN, 55905, USA

[2] Departments of Immunology and Laboratory Medicine/Pathology, Mayo Clinic, Rochester, MN, 55905, USA

[3] Department of Ophthalmology, Chinese PLA General Hospital, Beijing, 100853, China

[4] Department of Neuroscience, Mayo Clinic, Jacksonville, FL, 32224, USA

***Correspondence:**

Dr. Long-Jun Wu

Department of Neurology,

Mayo Clinic

200 First Street SW,

Rochester, MN 55905

TEL: (617) 943-7822

E-MAIL: wu.longjun@mayo.edu

Supplementary Figures and Figure Legends

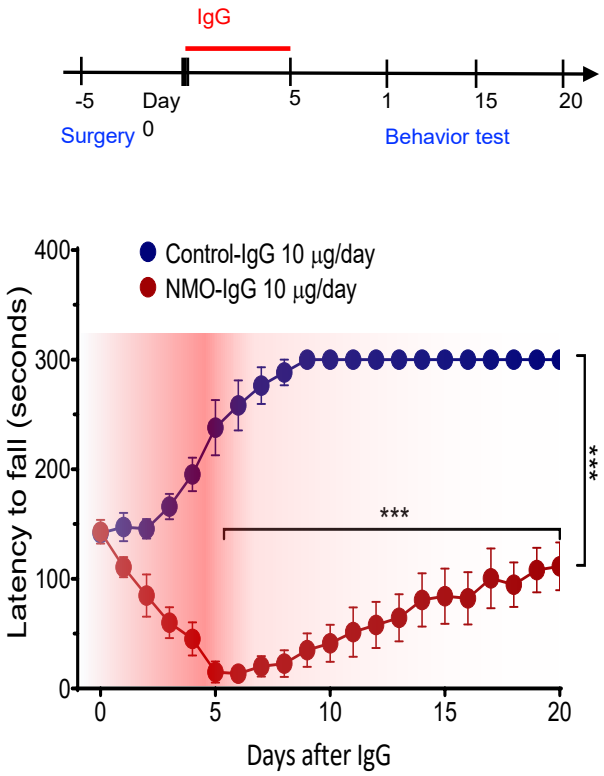

Figure S1. Early motor impairment induced by intrathecal infusion of NMO-IgG without exogenous complement is partially reversible.

(Upper) Timeline of experimental design. Rotarod tests show time-dependent motor impairment (measured as fall latency) resulting from 5 days' infusion of NMO-IgG, and motor function recovery upon cessation of IgG infusion. Data represent mean ± SEM, n = 4 in NMO-IgG and n = 3 in Control-IgG groups, Two-way ANOVA (NMO-IgG *vs.* control-IgG) and 2-tailed student's *t*-test (day 5 *vs.* day 20 in NMO-IgG group).*** $P < 0.001$.

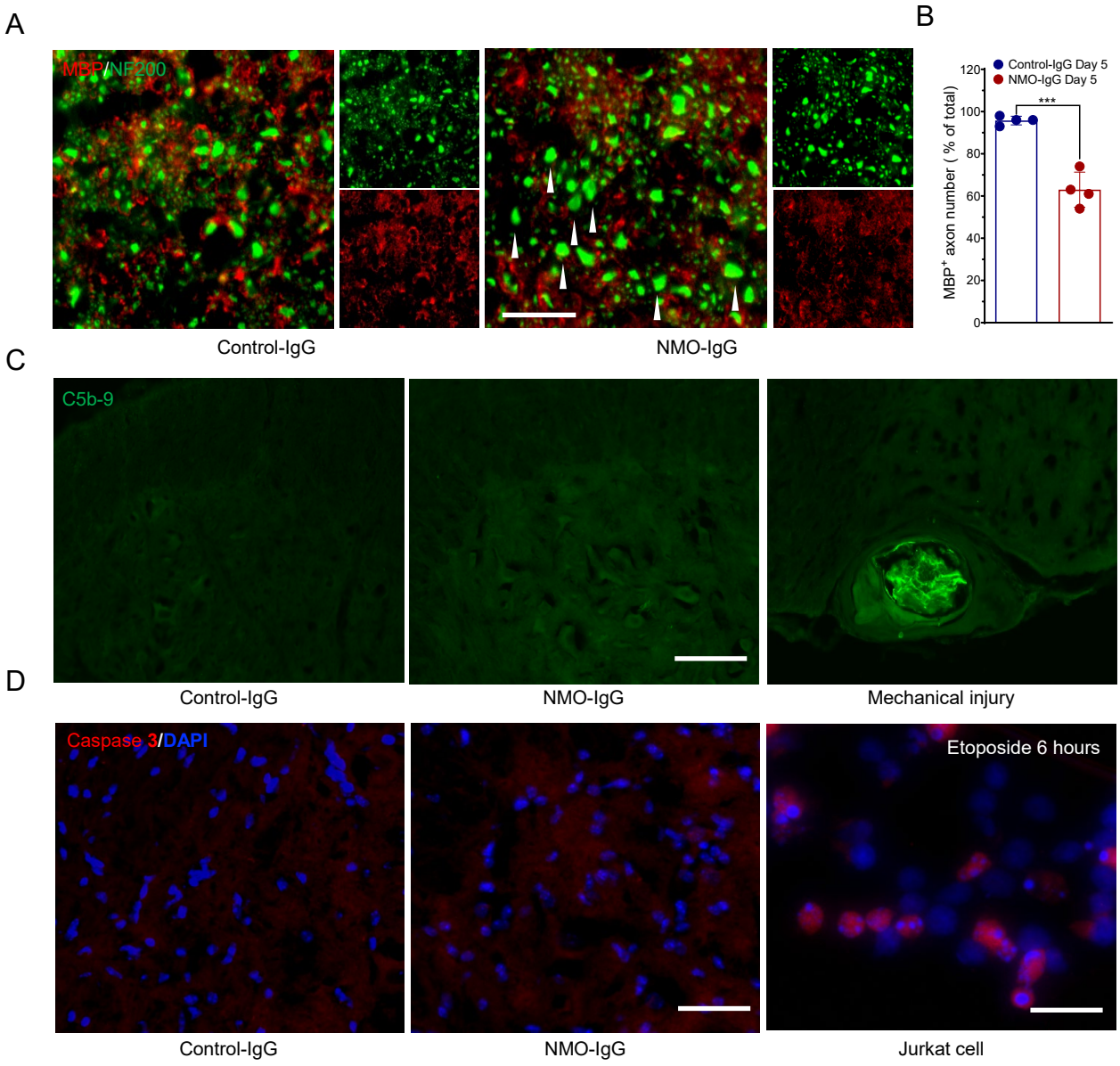

Figure S2. NMO-IgG infusion induces minor loss of myelin basic protein immunoreactivity without evidence of axonal damage, complement-mediated cell lysis or apoptosis.

(**A**) Representative spinal L4 cross sections show immunoreactivities of axoplasm (NF200, green) and myelin (MBP, red) on day 5 of IgG infusion (control or NMO), n = 4 mice (4 sections/mouse) in each group. Scale bar, 5 μm. (**B**) Bar graph shows relative

percentage of axon (NF200+) covered by MBP, which is significantly reduced in NMO-IgG recipients compared with control-IgG recipients, n = 4 mice (4 sections/mouse). (**C**) Representative spinal L4 cross sections show lack of the cytolytic membrane attack complex (C5b-9 immunoreactivity) in mice infused with either control-IgG (left) or NMO-IgG (middle); mechanically-injured mouse spinal cord (right) served as positive control for C5b-9 immunostaining, n = 4 mice (4 sections/mouse) in each group. Scale bar, 20 μm. (**D**) Representative spinal L4 cross sections lack cleaved Caspase 3 immunoreactivity (apoptosis marker) in mice infused with either control-IgG (left) or NMO-IgG (middle), n = 4 mice (4 sections/mouse) for each group. Scale bar, 20 μm; Jurkat cells treated with 40 mg/ml etoposide, 6 hours (right), served as positive control for Caspase 3 immunostaining, Scale bar, 10 μm. Data represent mean ± SEM. 2-tailed student's *t*-test (**B**). *** $P < 0.001$.

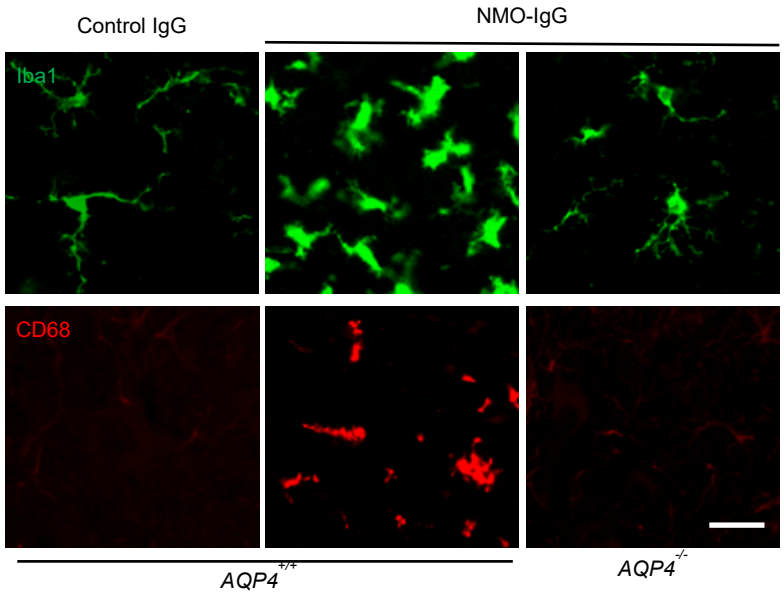

Figure S3. Microglial activation in NMO-IgG recipient mice is AQP4-dependent.

Lysosomal CD68 (red, lower) in Iba1+ microglia (green, upper) was upregulated in L4 spinal cord of wild-type (*Aqp4*$^{+/+}$) mice, but not in AQP4-null mice, on day 5 of NMO-IgG infusion. Wild-type recipients of control-IgG had low CD68 is expression, n = 5 mice (4 sections/mouse). Scale bar, 20 μm.

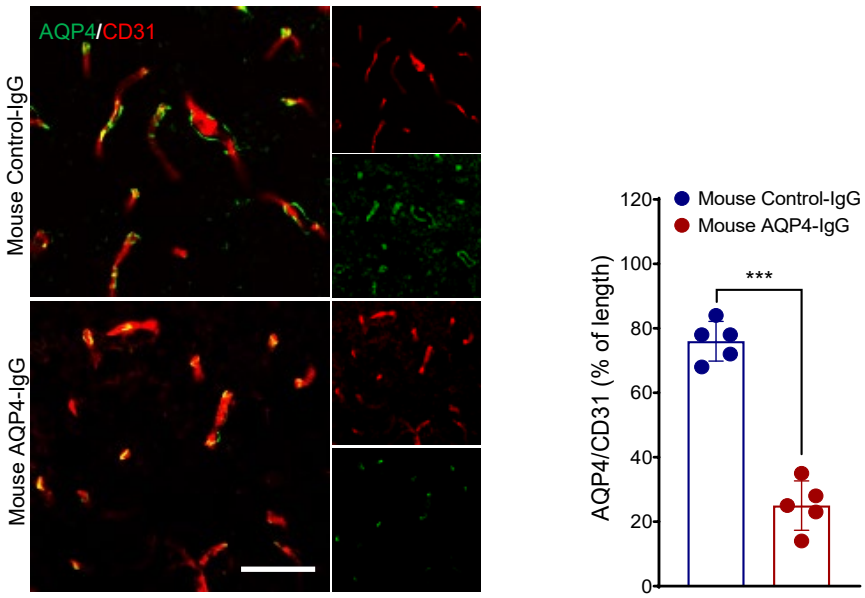

Figure S4. Mouse monoclonal AQP4-IgG induces AQP4 loss.

Representative spinal L4 cross sections show immunoreactivities of astrocytic AQP4 (green) and endothelial CD31 (red) on day 5 of mouse control-IgG infusion (upper) or monoclonal AQP4-IgG (lower). Scale bar, 20 μm. Bar graph shows quantitatively that relative length of AQP4-coverage of parenchymal blood vessels (CD31+) is significantly less in mouse AQP4-IgG recipient mice than in control-IgG recipients. n = 5 mice (4 sections/mouse). Data represent mean ± SEM, 2-tailed student's *t*-test. *** $P < 0.001$.

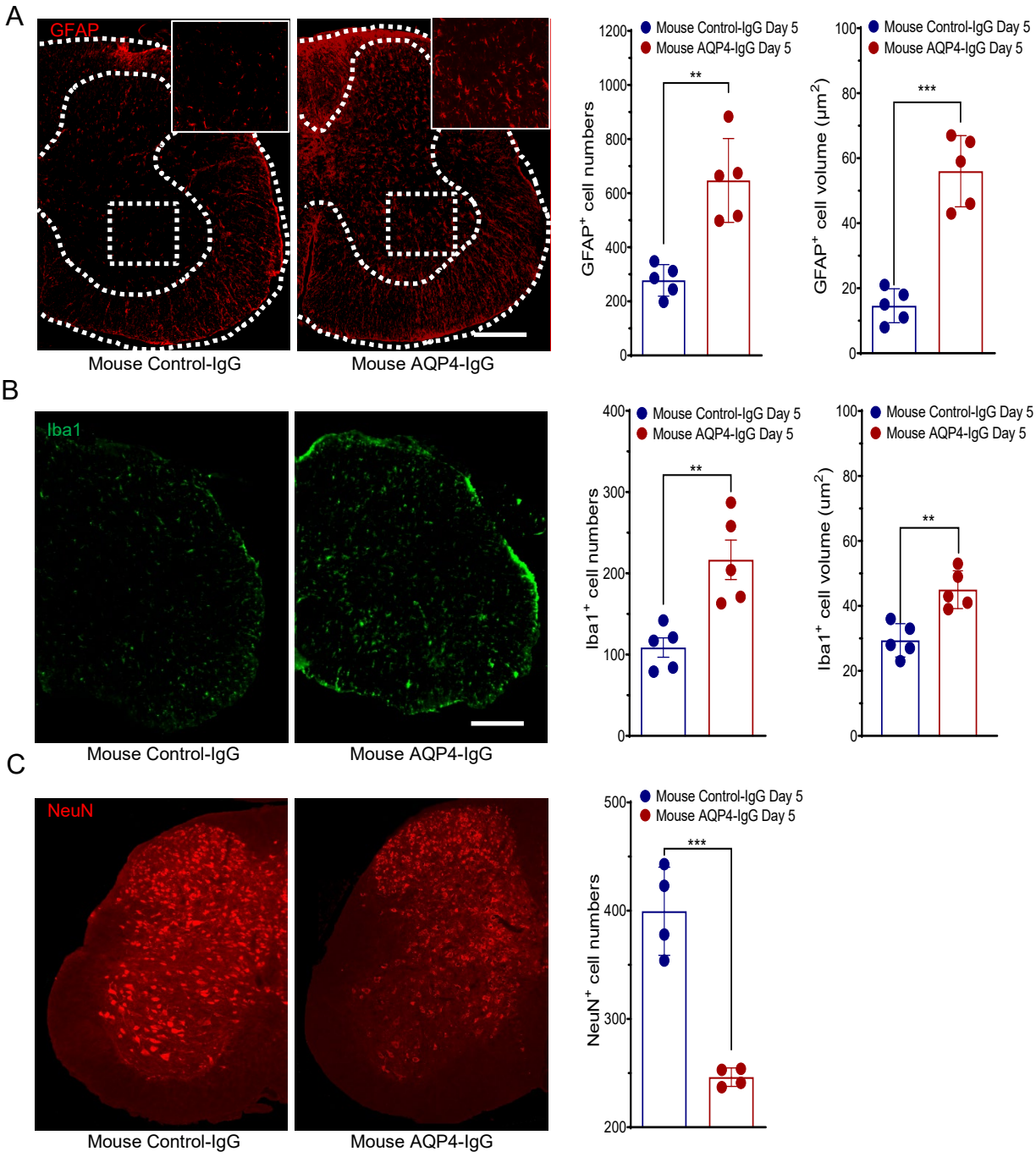

Figure S5. Astrocyte activation by mouse monoclonal AQP4-IgG leads to microglial activation and loss of neuronal NeuN.

Representative spinal L4 cross sections on day 5 of intrathecal IgG infusion (mouse control-IgG [left] or mouse monoclonal AQP4-IgG [right]) show (**A**) GFAP immunoreactivity; insets are higher magnifications of boxed areas in ventral horn. Bar graphs show that astrocyte relative numbers (left) and soma volumes (right) are both

significantly greater in AQP4-IgG recipient mice than in control-IgG recipients, n = 5 mice (4 sections/mouse). Scale bar, 200 μm. (**B**) Iba1 immunoreactivity. Bar graphs show that microglia relative numbers (left) and soma volumes (right) are both significantly greater in AQP4-IgG recipient mice than in control-IgG recipients, n = 5 mice (4 sections/mouse). Scale bar, 200 μm. (**C**) NeuN immunoreactivity. Bar graph shows that $NeuN^+$ cells are significantly fewer in AQP4-IgG recipient mice than in control-IgG recipients, n = 4 mice (4 sections/mouse). Scale bar, 200 μm. Data represent mean ± SEM, 2-tailed student's *t*-test (**A-C**). **P<0.01, *** P < 0.001.

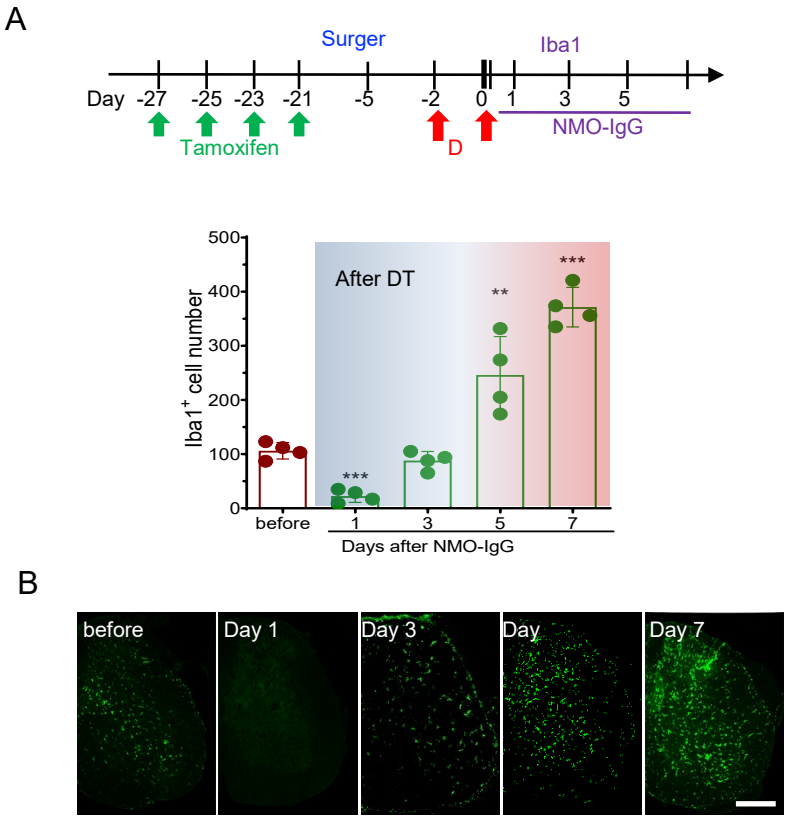

Figure S6. Time course of microglia depletion and replenishment after NMO-IgG infusion.

(**A**) (upper) Tamoxifen and diphtheria toxin (DT) were both injected *i.p.* starting, respectively, 1 month and 48 hours before continuous intrathecal IgG infusion began; mice were killed daily thereafter to enumerate L4 spinal cord microglia. (lower) Microglial numbers (Iba1$^+$) following DT administration and NMO-IgG infusion, n = 4 in each group. (**B**) Representative serial images of Iba$^+$ cells in L4 spinal cord cross sections, before and after diphtheria toxin administration, n = 4 mice (4 sections/mouse). Scale bar, 200 μm. Data represent mean ± SEM, one-way ANOVA (**A**). *** $P < 0.001$, ** $P < 0.01$.

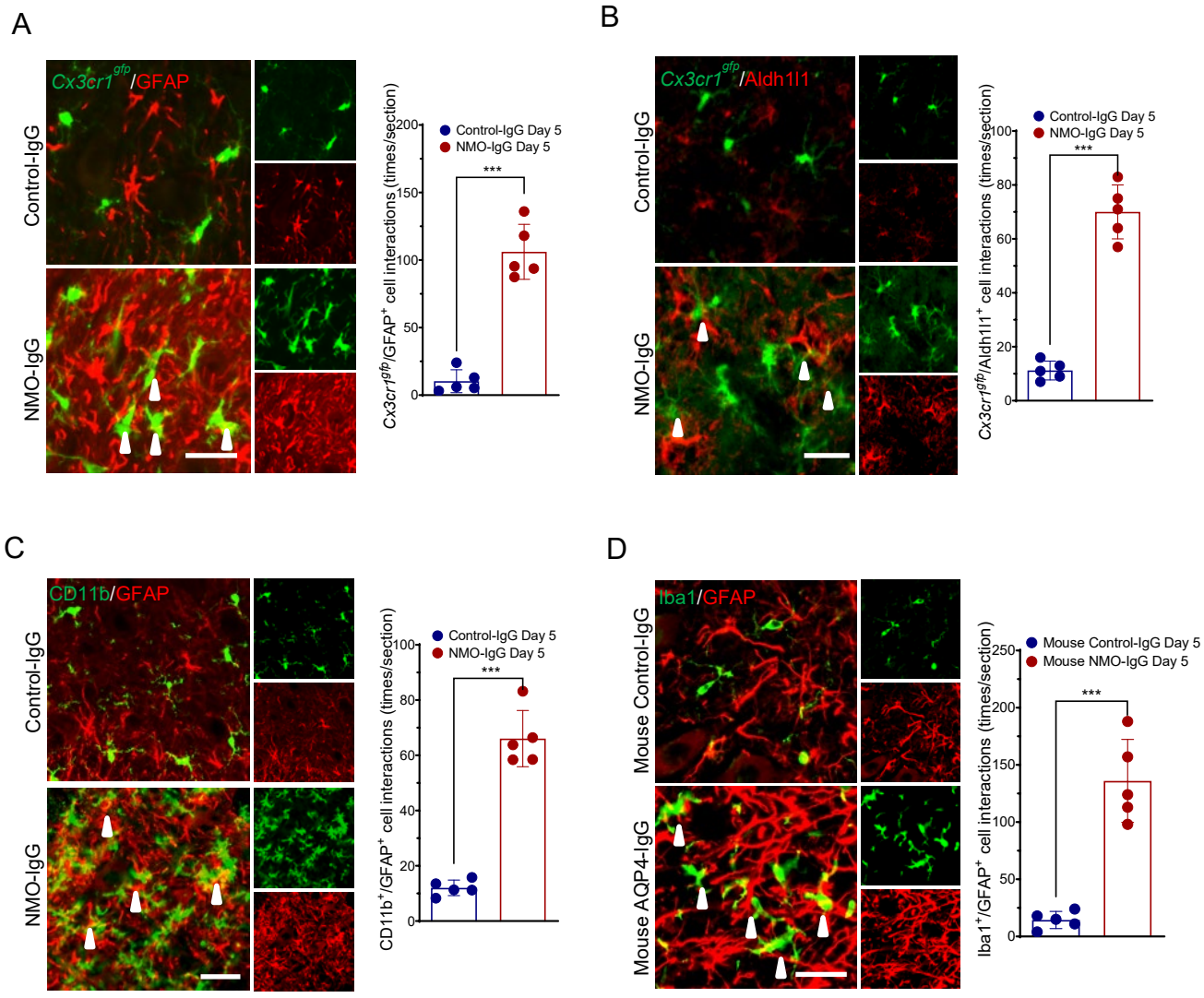

Figure S7. NMO-IgG induces astrocyte-microglia interactions.

(**A**) Interaction of *Cx3cr1*$^{gfp/+}$ microglia (green) and GFAP$^+$ astrocytes (red) is inferred from enlargement and overlapping of both cell types and their processes in dual immunostained L4 spinal cord of NMO-IgG-recipient mice compared with control-IgG recipients. Overlapping events quantified by ImageJ software, n = 5 mice (4 sections/mouse). Scale bar, 20 μm. (**B**) Representative images and bar graph quantification show interaction between *Cx3cr1*$^{gfp/+}$ microglia and Aldh1l1$^+$ (red)

astrocytes in NMO-IgG and control-IgG recipients, n = 5 mice (4 sections/mouse). Scale bar, 20 μm. (**C**) Astrocyte-microglia interaction was further confirmed by dual staining of $CD11b^+$ microglia (green) and $GFAP^+$ astrocytes (red), n = 5 mice (4 sections/mouse). Scale bar, 20 μm. (**D**) Mouse monoclonal AQP4-IgG, but not control-IgG, induced microglia-astrocyte interaction. Arrow heads indicate apparent overlaps of microglia and astrocytes, n = 5 mice (4 sections/mouse). Scale bar, 20 μm. Data represent mean ± SEM, 2-tailed student's *t*-test (**A**-**D**). *** $P < 0.001$.

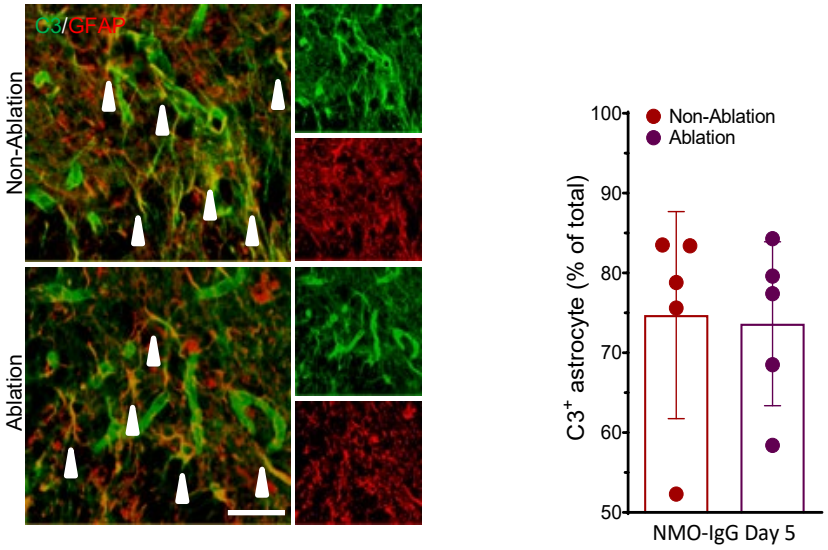

Figure S8. Genetic ablation of microglia did not prevent NMO-IgG-induced upregulation of astrocytic C3.

Dual staining reveals complement C3 (green) and GFAP (red) immunoreactivities in astrocytes of L4 spinal cord of mice at day 5 of NMO-IgG infusion, with and without microglia ablation. Arrow heads indicate co-localization of C3 and GFAP immunostaining. Scale bar, 20 μm. Bar graph quantifies $C3^+$ astrocytes in both ablation and non-ablation groups after NMO-IgG infusion, n = 5 mice (4 sections/mouse). Data represent mean ± SEM, 2-tailed student's *t*-test.

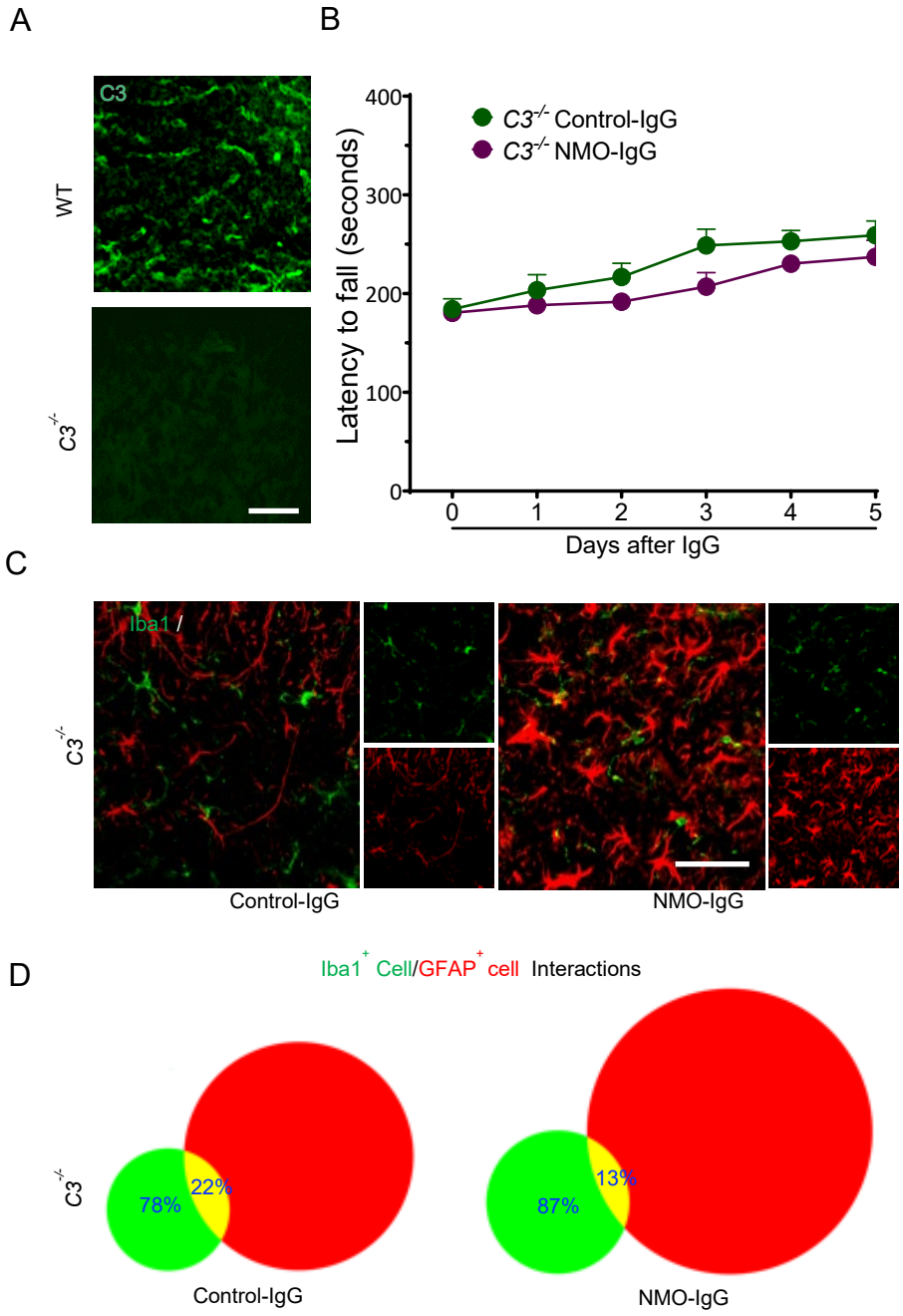

Figure S9. Signaling by early complement components is critical for initial NMO-IgG-induced motor impairment and progression of pathology.

(**A**) Spinal cord tissue of C3-null mice lacks C3 immunoreactivity (green) by comparison with wild-type mice, n = 4 mice (4 sections/mouse). Scale bar, 20 μm. (**B**)

Intrathecally-infused NMO-IgG did not significantly impair Rotarod performance of C3-null mice, n = 4 mice per group. (**C**) By comparison with control-IgG infusion, microglia ($Iba1^+$ cells) in L4 spinal cord of C3-null mice show no significant activation after NMO-IgG infusion, despite evidence of astrocyte activation (enlarged $GFAP^+$ cells), n = 4 mice (4 sections/mouse). Scale bar, 20 μm. (**D**) Microglia-astrocyte interaction events were quantified by ImageJ at day 5 of IgG infusion, n = 4 mice (4 sections/mouse). Data represent mean ± SEM, Two-way ANOVA (**B**).

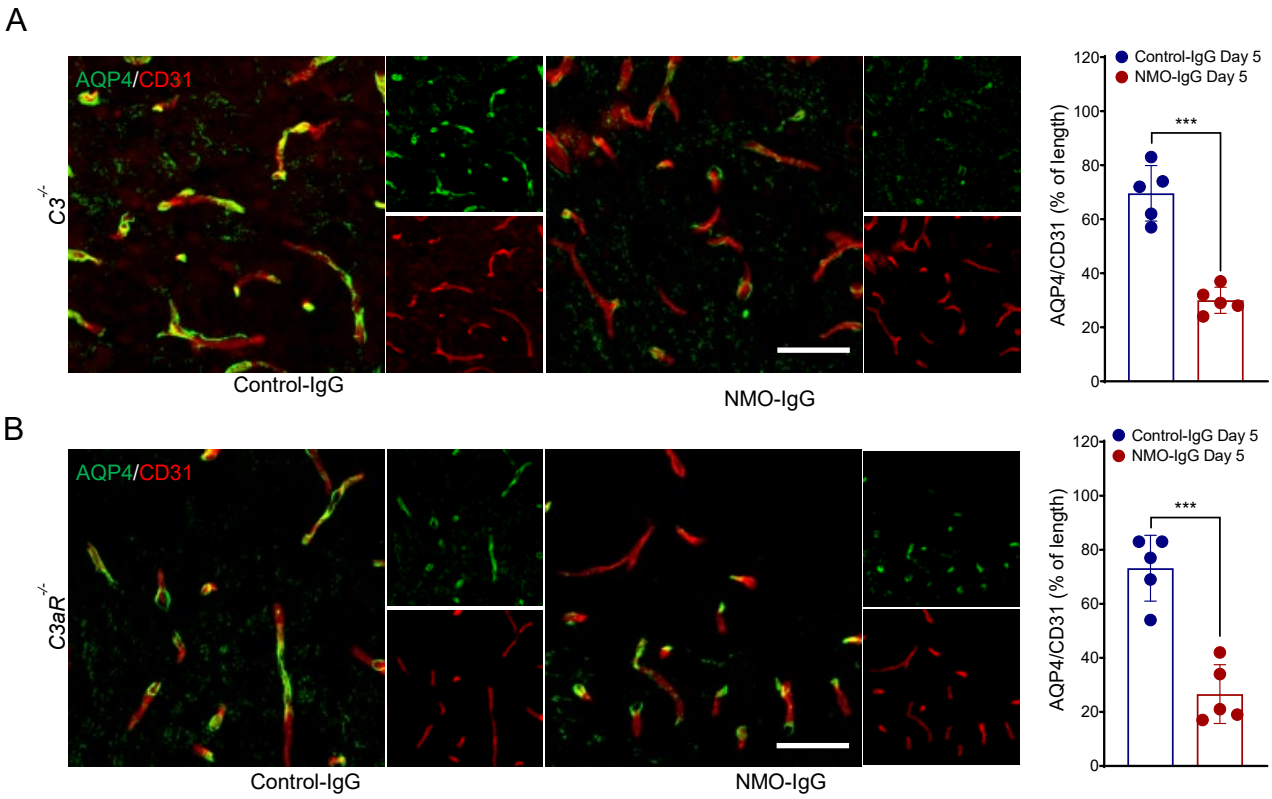

Figure S10. AQP4 is lost in both C3-null and C3aR-null mice after NMO-IgG infusion.

Representative images show astrocytic AQP4 (green) and endothelial CD31 (red) immunoreactivities after control-IgG (upper) or NMO-IgG (lower) in L4 spinal cord of mice lacking C3 (**A**) or C3a receptor (**B**), n = 4 mice in each group (4 sections/mouse). Scale bar, 20 μm. Bar graphs quantify the coverage of intraspinal blood vessels by AQP4, n = 4 mice (4 sections/mouse). Data represent mean ± SEM, 2-tailed student's *t*-test (**A-B**). ***P < 0.001.